Available online at www.sciencedirect.com
SCIENCE DIRECT®
Physica B 357 (2005) 39–44
PHYSICA B
www.elsevier.com/locate/physb

Heterodyne and homodyne detection in fluctuating smectic membranes by photon correlation spectroscopy at X-ray and visible wavelengths

Wim H. de Jeu[a,*], Anders Madsen[b], Irakli Sikharulidze[a], Samuel Sprunt[c]

[a]*FOM-Institute for Atomic and Molecular Physics, Kruislaan 407, 1098 SJ Amsterdam, The Netherlands*
[b]*ID10A, European Synchrotron Radiation Facility, BP 220, 38043 Grenoble, France*
[c]*Physics Department, Kent State University, Kent, OH 44204, USA*

Abstract

We discuss heterodyne and homodyne detection in photon correlation spectroscopy (PCS) performed at X-ray and visible wavelengths. Fluctuating smectic membranes in a reflection geometry have been used as model systems. At X-ray wavelength (XPCS), under specular conditions a strong elastic signal is present that acts as a time-independent internal reference source. This leads to a transition from heterodyne detection at the specular ridge to homodyne detection off-specular giving rise to a difference in relaxation time of a factor 2. In addition by comparing similar propagating modes at the specular ridge (XPCS) and at off-specular positions (PCS with visible light), cos-like and $\cos^2$-like oscillations have been observed as expected for heterodyne and homodyne mixing, respectively.

PACS: 42.25.Kb; 61.10.Kw; 61.30.−v

Keywords: Photon correlation spectroscopy; Coherent radiation; Smectic liquid crystals

1. Introduction

During the last decade the development of third-generation synchrotrons made it possible to extend photon correlation spectroscopy (PCS) from the optical region into the X-ray domain [1]. This allows to probe dynamics on molecular length scales as well as the use of optically dense samples inappropriate for conventional PCS. Using smectic membranes as model systems, X-ray photon correlation spectroscopy (XPCS) has been extended into the sub-microsecond range [2,3]. Smectic membranes [4] consist of stacks of liquid layers made up of elongated molecules with their principal axis oriented perpendicular to the layers. The nearly perfect alignment of the smectic

*Corresponding author. Tel.: +31 20 608 1315; fax: +31 20 668 4106.
E-mail address: dejeu@amolf.nl (W.H. de Jeu).

0921-4526/$ - see front matter © 2004 Elsevier B.V. All rights reserved.
doi:10.1016/j.physb.2004.11.016

structure by the surfaces allows us to obtain intense and narrow reflections. This property makes smectic membranes particularly suitable for use in a high-resolution PCS setup. The one-dimensional ordering of the smectic layers leads to strong fluctuations in the system. Defining $u(\mathbf{r})$ as the layer displacement from its equilibrium position, $\langle u^2(\mathbf{r})\rangle$ is found to diverge logarithmically with the sample size (Landau–Peierls instability) [5] finally destroying the ordering. However, the divergence is slow, which opens the possibility to prepare finite-size samples. These fluctuations generate 'undulations' on the surface of the membrane, which can be measured with PCS. More precisely the intensity scattered with a wave vector $\mathbf{q}$ is defined by the intermediate scattering function $S(\mathbf{q}, t)$, which is related to the layer-displacement correlation function $\langle u(\mathbf{r}_1, 0)u(\mathbf{r}_2, t)\rangle$. The various fluctuation regimes measured with XPCS have been discussed elsewhere [2,3]. In short at small wave vector $q_\perp$ of the fluctuations a complex surface relaxation mode is observed, combining exponential decay with oscillatory behaviour. Transitions from complex behaviour to simple exponential decay occur as a function of film thickness and of $q_\perp$, in agreement with theory. Technical aspects have been discussed in Ref. [6]. In measuring the correlation function as a function of $q_\perp$ we observed a transition from heterodyne detection at the specular position to homodyne detection off-specular. In this paper, we discuss various aspects of these different detection schemes in some detail comparing also XPCS with PCS at visible wavelengths.

2. Photon correlation spectroscopy

PCS experiments are based upon optical mixing schemes [7,8] in which the scattered intensity $I(\mathbf{q}, t) = |E(\mathbf{q}, t)|^2$ at wave vector $\mathbf{q}$ and time t is measured by a detector and fed into a hardware autocorrelator that computes the normalized intensity correlation function

$$g_2(\mathbf{q}, \tau) = \frac{\langle I(\mathbf{q}, t)I(\mathbf{q}, t+\tau)\rangle}{\langle I(\mathbf{q}, t)\rangle^2}. \quad (1)$$

Similarly, we can define

$$g_1(\mathbf{q}, \tau) = \frac{\langle E(\mathbf{q}, t)E^*(\mathbf{q}, t+\tau)\rangle}{\langle I(\mathbf{q}, t)\rangle}. \quad (2)$$

The wave field $E(\mathbf{q}, t)$ scattered from a particular coherence volume interferes with itself but not with the field originating from neighbouring volume elements. As a result we can represent the scattering intensity as a sum of intensities scattered by each coherence region. Each component is related to the structure within the coherence volume and if this structure is changing in time the scattered intensity will also exhibit a time dependence. On the basis of this approach we can express the scattered intensity and the intensity correlator of Eq. (1) as (suppressing $\mathbf{q}$ for the moment)

$$\langle I(t)\rangle = \sum_{i=1}^{M} \langle I_i(t)\rangle,$$

$$\begin{aligned}\langle I(t)I(t+\tau)\rangle &= \Big\langle \sum_{i,j=1}^{M} I_i(t)I_j(t+\tau)\Big\rangle \\ &= \sum_{i=1}^{M} \langle I_i(t)I_i(t+\tau)\rangle, \\ &\quad + \sum_{i=1}^{M} \langle I_i(t)\rangle \sum_{j=1}^{M} \langle I_j(t)\rangle, \end{aligned} \quad (3)$$

where M is the number of coherence regions. Furthermore, we used the property that the scattered intensities from different coherence volumes are not correlated and $\langle I_i(t)I_j(t+\tau)\rangle = \langle I\rangle^2$ if $i \neq j$. According to Eq. (3) both $\langle I(t)I(t+\tau)\rangle$ and $\langle I(t)\rangle$ increase proportionally to the number of coherence volumes in the scattering region. Consequently $g_2(\tau)$ will decrease if the number of coherence volumes increases. Maximum performance is achieved for a spatially highly coherent beam in which the coherence and the scattering volume match.

In optical mixing experiments we can distinguish homodyne and heterodyne detection schemes. The homodyne mode works with a superposition of the scattered fields $E(\mathbf{q}, t) = \sum E_s(\mathbf{q}, t)$. The intensity–intensity autocorrelation function is determined by the second-order correlation function

$\langle \rho(\mathbf{q},0)\rho^*(\mathbf{q},0)\rho(\mathbf{q},\tau)\rho^*(\mathbf{q},\tau)\rangle$ of the Fourier transform of the electron density $\rho(\mathbf{q},t)$. However, note that the first-order correlation function $\langle \rho(\mathbf{q},0)\rho^*(\mathbf{q},\tau)\rangle$ is directly related to the intermediate scattering function through Fourier transformation. If the fields $E_s(\mathbf{q},t)$ are statistically independent random variables, $E(\mathbf{q},t)$ will follow a Gaussian distribution that is completely characterized by its first and second moment. This implies that for the homodyne scheme the 4-field intensity correlator in $g_2(\mathbf{q},t)$ can be expressed through the 2-field correlator in $g_1(\mathbf{q},\tau)$ as

$$g_2(\mathbf{q},\tau) = 1 + |g_1(\mathbf{q},\tau)|^2. \tag{4}$$

This expression is known as the Siegert relation. A direct consequence of this equation is that $g_2(\tau)\geqslant 1$. In the overdamped situation $g_1(\mathbf{q},\tau)$ follows an exponential decay with a relaxation rate Γ and from Eq. (4) we can write

$$g_2(\mathbf{q},\tau) = 1 + \beta_{\mathrm{hom}} \exp(-2\Gamma\tau). \tag{5}$$

For propagating modes one observes an exponentially damped oscillation of the correlation function given by

$$g_2(\mathbf{q},\tau) = 1 + \beta_{\mathrm{hom}} \cos^2(\omega\tau)\exp(-2\Gamma\tau). \tag{6}$$

In the heterodyne scheme the fluctuating field $E_s(\mathbf{q},t)$ from the sample is mixed with a static reference field $E_{\mathrm{ref}}(\mathbf{q})$. This field does not depend on time and can interfere with $E_s(\mathbf{q},t)$ from the sample: $E(\mathbf{q},t) = E_{\mathrm{ref}}(\mathbf{q}) + E_s(\mathbf{q},t)$. The intensity–intensity correlator can now be written in the form

$$\langle I(\mathbf{q},t)I(\mathbf{q},t+\tau)\rangle \sim 2(I_s I_{\mathrm{ref}})\mathrm{Re}[g_1(q,\tau)] + I_s^2 g_2(\mathbf{q},\tau). \tag{7}$$

In the situation $I_{\mathrm{ref}} \gg I_s$ this leads to the following result for the normalized intensity–intensity correlation function:

$$g_2(\mathbf{q},\tau) \approx 1 + 2(I_s/I_{\mathrm{ref}})\mathrm{Re}[g_1(\mathbf{q},\tau)]. \tag{8}$$

In the overdamped situation we now find

$$g_2(\mathbf{q},\tau) = 1 + \beta_{\mathrm{het}} \exp(-\Gamma\tau). \tag{9}$$

The equivalent result for the propagating mode is

$$g_2(\mathbf{q},\tau) = 1 + \beta_{\mathrm{het}} \cos(\omega\tau)\exp(-\Gamma\tau). \tag{10}$$

Note that $\beta_{\mathrm{het}}/\beta_{\mathrm{hom}} = 2I_s/I_{\mathrm{ref}}$; hence control of this ratio is of the most importance. Compared to the homodyne regime several points are remarkable. First we observe in the heterodyne regime $g_1(\tau)$ and not its square. This results in a factor 2 difference between the (exponential) relaxation times observed in homodyne and heterodyne detection schemes [9], and to a $\cos^2$ and a cos-behaviour, respectively, for the oscillations in the propagating case. Second we note from Eq. (7) that the intensity of the local oscillator amplifies the contribution of the weakly scattered signal. However, Eq. (8) indicates that this increase in intensity goes at the expense of a decrease in contrast of the correlation function. For PCS with visible light, coherent lasers are available and contrast is not of primary concern. Hence, often a special grating is placed in the beam to create a strong secondary source, and heterodyne detection is the preferred choice. Summarizing, we can say that homodyne detection gives maximum contrast (other factors being constant) but less intensity while heterodyne mixing gives a larger fluctuating intensity but lower contrast.

The static reference field does not necessarily have to be external but can come from the sample itself [3,10]. If we can separate the scattered intensity from the sample into a time-dependent and a time-independent part, similar arguments can be applied as used above. The scattered field and the electron-density profile of the sample are linearly correlated, which can be expressed in the form

$$E(\mathbf{q},t) = \int \mathrm{d}\mathbf{r}\rho(\mathbf{r},t)R(\mathbf{q},\mathbf{r})\mathrm{e}^{-\mathrm{i}(\mathbf{q}\cdot\mathbf{r})}, \tag{11}$$

where $R(\mathbf{q},\mathbf{r})$ includes resolution-dependent factors and possible Fresnel corrections [11]. If we split the density into a time-dependent and a time-independent part $\rho(\mathbf{r},t) = \rho_0(\mathbf{r}) + \Delta\rho(\mathbf{r},t)$, we can decompose the scattered field $E(\mathbf{q},t)$ into two components. The first part is defined by the average distribution of the scatterers and thus will be time-independent. The second term accounts for the deviation of the scatterers from their average positions, resulting in the time-dependent component. Obviously the two

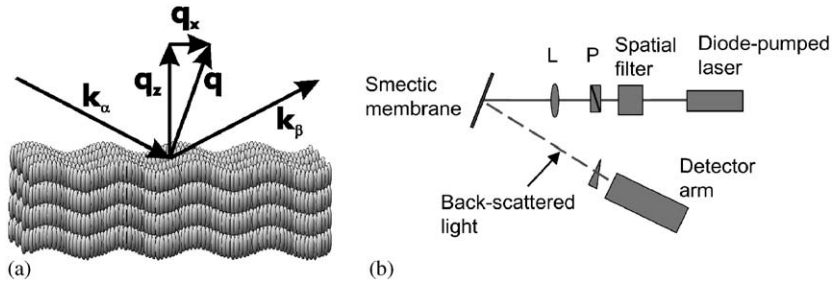

Fig. 1. Scattering geometry for (a) XPCS with X-rays at beamline ID10 of ESRF, (b) Schematic setup of PCS at visible wavelength.

components interfere with each other thus fulfilling the requirements for heterodyne detection.

3. Experimental

We studied smectic-A membranes of the compound 4-octyl-4'-cyanobiphenyl (8CB) around room temperature at 25–27 °C (smectic-A–nematic transition temperature $T_{AN} = 33.5\,^{\circ}C$). For XPCS, membranes were stretched to about $15 \times 5\,mm^2$ using a stainless-steel frame with movable blades [3]. X-ray scattering experiments were performed at the undulator beamline ID10A (Troïka I) of the European Synchrotron Radiation Facility (ESRF, Grenoble, France), as described in more detail elsewhere [3]. In short, membranes were mounted vertically in a reflection geometry (see Fig. 1a) and illuminated with 13.4 keV radiation ($\lambda = 0.09\,nm$) using a 10-μm pinhole. Measurements were performed in the uniform filling mode of the storage ring (992 bunches at intervals of 2.8 ns). A fast avalanche photodiode (Perkin-Elmer C30703) with an intrinsic time resolution $\lesssim 2\,ns$ was used as detector. The coherent photon flux at the sample was about 10^8 counts $s^{-1}/100\,mA$. The intensity–intensity time auto-correlation function was computed in real time using a hardware multiple-tau digital auto-correlator FLEX01-8D (correlator.com, sampling time down to 8 ns). At the Bragg position, MHz count rates were reached that allowed measurements as a function of the wavelength of the fluctuations at off-specular positions ($q_\perp \neq 0$) (see Fig. 1a).

PCS on 8CB was done using the setup depicted in Fig. 1b. A focused 532 nm laser beam (polarized vertical to the scattering plane) illuminated the film at an incident angle $\theta_i = 27^{\circ}$ (relative to the film normal), and vertically polarized scattering was collected at a scattering angle $|\theta_s - \theta_i| = 3.5^{\circ}$. A 50/50 beamsplitter divided the scattered light between two photomultiplier modules (Hamamatsu HC120-08), whose outputs were cross-correlated. Homodyne correlation functions were computed by a home-built digital correlator, which features a fast section composed of 32768 channels at 1 ns spacing. Typical scattering intensities were 100 kHz for incident laser powers of several mW.

4. Results and discussion

As discussed above, the density of a fluctuating smectic membrane can be decomposed into a time-independent (average) part and a time-dependent one. The field $E_s(\mathbf{q}, t)$ accounts for the deviation of the scatterers from their average positions reflected in $E_{ref}(\mathbf{q})$, resulting in the time-dependent component. At the quasi-Bragg position (or more general at the specular ridge) a strong elastic component is present that acts as a static reference field. Then the dominant term in the correlator is the cross product of this elastic and the quasi-elastic component. As a result, in this heterodyne detection scheme only one component of the correlator carries the time dependence and we measure Γ directly. At far off-specular positions we do not catch the static component and we are dealing with homodyne detection. In this regime, calculation of the corresponding correlator leads to an experimental relaxation time 2Γ.

Fig. 2 shows some typical experimental XPCS results for 8CB. Around the quasi-Bragg position we observe a specular relaxation time of 6.2 μs. After passing a threshold the correlation function transforms to a different relaxation time. This transition manifests the switch between homodyne and heterodyne detection schemes as the contribution of I_{ref} disappears. The threshold is determined by the angle for which the specular reflection falls on the edge of the detector area. The results in Fig. 2 indicate an off-specular relaxation time of 3.3 μs. The experimental ratio of 1.9 is very close to the expected factor 2 and nicely confirms the transition from heterodyne to homodyne detection. The prediction of a higher contrast in the homodyne case is not borne out. This is not so surprising as several other factors influence the contrast like the number of coherence regions, compare Eq. (3). Moreover, in this particular case of smectic membranes the fluctuating intensity decreases upon approaching $q_z = 0$.

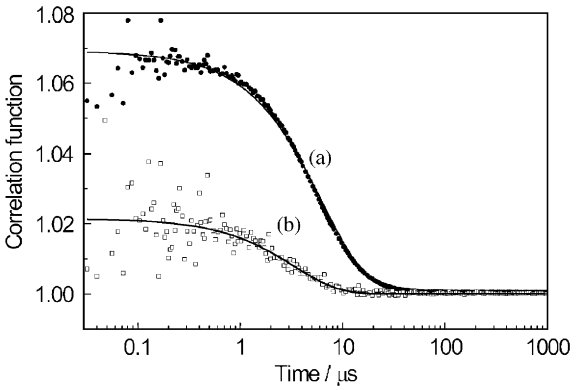

Fig. 2. XPCS measurements of a 3.8 μm 8CB membrane at (a) the specular Bragg position ($\tau = 6.2\,\mu s$) and (b) off-specular at $q_\perp = 5.2 \times 10^{-3}\,nm^{-1}$ ($\tau = 3.3\,\mu s$).

Fig. 3a gives specular XPCS data for a thinner 8CB sample that shows in addition to the exponential decay oscillations (propagating mode). The intensity alternates around the baseline and hence can be described by a cos-form. From the discussion above this is as anticipated for heterodyne detection at the specular ridge. In contrast Fig. 3b shows a propagating mode of 8CB from visible light scattering, which in this situation is taken at an off-specular angle of 3.5° (homodyne). Indeed now the oscillations stay above the baseline ($\cos^2$-behaviour) indicating homodyne detection in agreement with our earlier discussion.

In conclusion, by PCS at X-ray and visible wavelength we have observed both heterodyne and homodyne detection in fluctuating smectic membranes in a reflection geometry. Clear evidence has been provided for a transition in XPCS between heterodyne detection at the specular ridge and homodyne detection for off-specular scattering geometries. In particular a difference in relaxation time of a factor 2 is found as expected. In addition, by comparing propagating modes at the specular ridge (XPCS) and at off-specular positions (PCS with visible light), cos-like and $\cos^2$-like oscillations have been observed as expected for heterodyne and homodyne mixing, respectively. For XPCS heterodyning occurs because of a strong elastic signal present at the specular ridge that acts as a time-independent internal reference source.

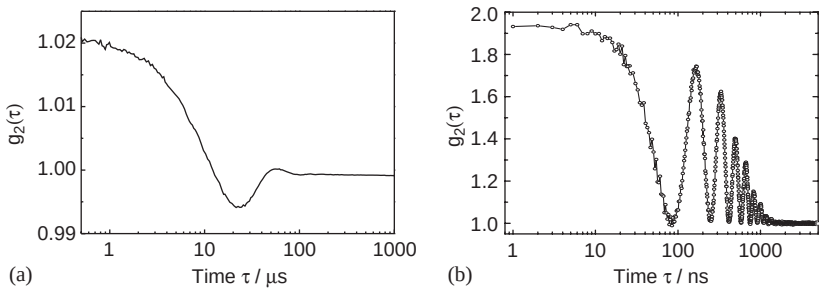

Fig. 3. Correlation functions of an underdamped mode showing oscillations. (a) XPCS of a 2.5 μm thick 8CB membrane at the specular Bragg position (heterodyne). (b) PCS of a 0.1 μm thick 8CB membrane at a wavelength of at 532 nm and an off-specular position $|\theta_s - \theta_i| = 3.5°$ (homodyne).

Acknowledgements

The authors thank Igor Dolbnya (Grenoble) for taking part in the XPCS measurements. This work is part of the research program of the 'Stichting voor Fundamenteel Onderzoek der Materie' (FOM), which is financially supported by the 'Nederlandse Organisatie voor Wetenschappelijk Onderzoek' (NWO). S. Sprunt was supported by the National Science Foundation under Grant no. DMR99-04321.

References

[1] S. Dierker, NSLS Newsletter, July, 1 (1995);
D.L. Abernathy, et al., J. Synchrotron Radiat. 5 (1998) 37;
D. Lumma, L.B. Lurio, S.G.J. Mochrie, M. Sutton, Rev. Sci. Inst. 71 (2000) 3274;
T. Seydel, A. Madsen, M. Sprung, M. Tolan, G. Grübel, W. Press, Rev. Sci. Inst. 74 (2003) 4033;
M. Sutton, K. Laaziri, F. Livet, F. Bley, Opt. Express 11 (2003) 2268;
G. Grübel, F. Zontone, J. Alloys Compounds 362 (2004) 3.

[2] A.C. Price, L.B. Sorensen, S.D. Kevan, J. Toner, A. Poniewierski, R. Hołyst, Phys. Rev. Lett. 82 (1999) 755;
A. Fera, I.P. Dolbnya, G. Grübel, H.G. Muller, B.I. Ostrovskii, A.N. Shalaginov, W.H. de Jeu, Phys. Rev. Lett. 85 (2000) 2316.

[3] I. Sikharulidze, B. Farago, I. Dolbnya, A. Madsen, W.H. de Jeu, Phys. Rev. Lett. 91 (2003) 165504;
I. Sikharulidze, I.P. Dolbnya, A. Fera, A. Madsen, B.I. Ostrovskii, W.H. de Jeu, Phys. Rev. Lett. 88 (2002) 115503.

[4] W.H. de Jeu, B.I. Ostrovskii, A.N. Shalaginov, Rev. Mod. Phys. 75 (2003) 181 and references therein.

[5] See, for example, P.M. Chaikin, T.C. Lubensky, Principles of Condensed Matter Physics, Cambridge University Press, Cambridge, UK, 1995.

[6] I. Sikharulidze, I.P. Dolbnya, A. Madsen, W.H. de Jeu, Opt. Commun. in press.

[7] See, for example, B. Chu, Laser Light Scattering: Basic Principles and Practice, Academic Press, San Diego, USA, 1991.

[8] B. Berne, R. Pecora, Dynamic Light Scattering with Applications to Chemistry, Biology and Physics, Dover Publications Inc., New York, 2000.

[9] D. Langevin (Ed.), Light Scattering by Liquid Surfaces and Complementary Techniques, New York, Dekker, 1992.

[10] C. Gutt, T. Ghaderi, V. Chamard, A. Madsen, T. Seydel, M. Tolan, M. Sprung, G. Grübel, S.K. Sinha, Phys. Rev. Lett. 91 (2003) 076104 (erratum: ibid 92 (2004) 096104).

[11] S.K. Sinha, M. Tolan, A. Gibaud, Phys. Rev. B 57 (1998) 2740;
M. Tolan, T. Seydel, A. Madsen, G. Grübel, W. Press, S.K. Sinha, Appl. Surf. Sci. 182 (2001) 236.